ORIGINAL PAPER

Synthesis of micro-FeTi powders by direct electrochemical reduction of ilmenite in CaCl$_2$-NaCl molten salt

Zhongren Zhou[1,2] · Yixin Hua[1,2] · Cunying Xu[1,2] · Jian Li[1,2] · Yan Li[1,2] · Qibo Zhang[1,2] · Yadong Zhang[1,2] · Wenhao Kuang[1,2]

Abstract Micro-ferrotitanium powders have been prepared by molten salt electrolysis via directly electrochemical reduction of solid ilmenite in eutectic CaCl$_2$-NaCl melt at 973 K. In the direct electrochemical reduction process, the reduction of FeTiO$_3$ first gives rise to the formation of Fe and CaTiO$_3$, which as intermediates will be further deoxidized at the interface of iron metals, solid CaTiO$_3$ matrix, and electrolyte to directly form ferrotitanium alloy powders in porous structure. Furthering the electrolytic time can promote the dense structure of ilmenite pellet turn to be more porous, indicating pores inside the pellet are sufficient for the diffusion of oxygen ions. Based on the reduction behavior of partially reduced powders in metallic cavity electrode during the cathodic potentiostatic electrolysis, it shows that the slow deoxidization rate is mainly caused by the more and more difficult reduction of CaTiO$_3$ than that of FeTiO$_3$.

Keywords Micro-ferrotitanium powders · Ilmenite · Molten salt electrolysis · Reduction mechanism

Introduction

In recent years, the direct extraction of metals and alloys in solid state from their complex multicomponent oxide powders

✉ Yixin Hua
yxhua@kmust.edu.cn

1 Faculty of Metallurgical and Energy Engineering, Kunming University of Science and Technology, Kunming 650093, People's Republic of China

2 Present address: State Key Laboratory of Complex Nonferrous Metal Resources Clean Utilization, Kunming 650093, People's Republic of China

with anisotropic particle morphologies has attracted considerable attentions by molten salt electrolysis method [1–4]. This method is actually an electrolytic process in molten salt by using the graphite as consumable anode and the sintered compounds pellet that is tied to a noble electrode as cathode. During electrolysis, oxygen in solid oxides is gradually ionized and dissolved into electrolyte, which is then discharged to form CO and CO$_2$ at the graphite consumable anode [5]. This method is well known as the Fray-Farthing-Chen (FFC) Cambridge electro-deoxidization process and has been applied to convert metallic oxides directly into metals and alloys in solid state successfully due to the advantage of the crystal growth at temperatures far below the melting point of the synthetic product phase, such as Nb, Ta, Ti, Ge, NiTi, and ZrSi alloy powders [6–9]. Contrary to the previous attempts including the dissolution of the mineral and the deposition of the metal, the FFC Cambridge process provides an effective metallurgical process that the porous mineral precursor is simply "metallized" in solid state on the cathode with the aid of molten salts, offering advantages in both case of operation and economics over metallothermic reduction [10, 11]. The as-produced metals from the FFC Cambridge process also retrain the shape of the mineral precursor with some shrinkage in dimensions. Thus, it is possible to control the process conditions to produce the powdery, porous, or dense metal products for the industrial demand. This method has also been carried out on pilot scale at the company Metalysis (https://www.metalysis.com) in England.

Ferrotitanium, used as a well-known hydrogen-storage carrier and deoxidizer, is traditionally prepared by carbothermic and aluminothermic reduction of oxide ores and concentrates or by melting iron and titanium scraps together at high temperatures. However, these methods have many disadvantages such as high-energy consumption and low quality of products. For example, the carbothermic process should be operated in

an electric arc furnace at extremely high temperatures, which leads to not only an extensive energy consumption but also a high carbon residue in the FeTi products. The aluminothermic process consumes a large quantity of aluminum primarily for maintaining a sufficient heat balance, and the energy consumption of this technique is regrettably also high.

The FFC process provides a promising technique for the extraction of FeTi alloy powders from their oxides, such as ilmenite ores and titanium slag [12–15]. Recently, researchers have prepared FeTi alloys with this process at 1223 K by use of the pretreated ferrotitanium oxide processor as cathode, graphite as the consumable anode, and $CaCl_2$ as electrolyte. Eventually, they found that some intermediates such as $CaTiO_3$, TiO_2, and TiO were produced during electrolysis [16–19], and the electrochemical reduction path was indicative to be a stepwise process. However, we found that ferrotitanium alloys were produced by the direct electro-deoxidization of perovskite in the presence of metallic iron-enriched grains other than producing sub-titanium oxides. The further deoxidization of perovskite also left plenty of pores and led into forming micro-ferrotitanium alloy powders in porous structures. Thus, more investigations and comprehensive measurements are needed to better understand the phase transitions as well as the mass transfer mechanisms.

This study provides compelling evidence for the electrochemical extraction of ferrotitanium alloy powders directly from ilmenite by using ilmenite as cathode, graphite as consumable anode, and equal molar eutectic $CaCl_2$-NaCl as electrolyte at 973 K. The reduction path was investigated by cathodic linear sweep voltammetry, potentiostatic electrolysis, and constant cell voltage electrolysis. The morphology of the reduced pellet was observed by second electron morphology (SEM), back-scattered electron (BSE), and energy-dispersive spectroscopy (EDS), respectively.

Experimental

Preparation of $CaCl_2$-NaCl eutectic electrolyte

The analytical grade anhydrous $CaCl_2$ (73 g, purity >97 mass%) and NaCl (32 g, purity >98 mass%) were mixed at equal molar ratio, added into a Al_2O_3 crucible (57 mm in inner diameter, 63 mm in outer diameter, and 75 mm in depth) and transferred into a vertical quartz tube reactor under argon (analytical grade, >99.999 %). The mixture was heated to 973 K that was higher than the eutectic point of 777 K [20]. Pre-electrolysis was carried out at 2.8 V for 12 h by using the graphite (99.9 % in purity, 6 mm in diameter, and 80 mm in length) as anode and molybdenum plate (10 × 10 mm) as cathode in order to remove redox-active impurities remained in molten salt.

Electrochemical analysis

All electrochemical measurements were carried out under a purified argon atmosphere in eutectic $CaCl_2$-NaCl melt at 973 K by using a computer-controlled CHI760D electrochemical system (Shanghai Chenhua, China). A conventional three-electrode cell was used for these experiments. A metallic cavity electrode (MCE) [21] filled with/without $FeTiO_3$ powders (particle size ~50 μm) was served as the working electrode, a graphite stick (99.9 % in purity, 2 mm in diameter, and 100 mm in length) as the counter electrode, and an Ag wire (0.5 mm in diameter and 50 mm in length) as the quasi-reference electrode. The mass of ilmenite powders in MCE was measured about 0.006 g. Generally, the metallic cavity electrode (MCE) has been employed comprehensively in the electrochemical analysis [22–27] due to the characteristics of the tiny iR drop and high CV measurements sensitivity. In the present study, the MCE was fabricated by high-speed mechanical drilling a ~0.35-mm circular hole at the end of molybdenum foil (0.5-mm thickness, ~0.7-mm width, and ~100-mm length). The foil was then polished on the metallographic sandpaper, boiled in concentrated NaOH for another 10 min, washed in distilled water, and dried in air. Then, micro-$FeTiO_3$ powders were manually filled into the MCE hole by repeatedly finger-pressing the powder on both sides of the foil, and wiped off carefully any powder left on the surface of the foil.

In the current experiment, ilmenite powders filled into the MCE hole were first immersed into the molten salt for 5 h without electrolysis to investigate the phase changes. After that, linear cathodic sweep voltammetry and chronoamperometry of $FeTiO_3$-MCE were measured with the starting potential of 0.05 V (vs. Ag), which was more negative than the open circuit potential of 0.10 V (vs. Ag). After cathodic potentiostatic electrolysis at −0.8 V for 5 min, 60 min and at −1.5 V for 5 min and 60 min, the reduced powders in MCE were removed from the cavity, washed with distilled water in order to remove residual salts, and then examined by X-ray diffraction (D/max-2200pc model) with Cu K-alpha radiation at a scan rate of 10°/min in the range of $2^\theta = 10 \sim 90°$.

Products and morphology analysis after electrolysis

In order to verify the reduction mechanism, electrolytic experiments were carried out in the two-electrode cell between assembled $FeTiO_3$ pellet cathode and graphite anode for 2 ~ 16 h at cell voltage of 3.2 V under argon inert atmosphere. The schematic diagram of experimental apparatus and the assembled ilmenite cathode were shown in Fig. 1. The cathode was assembled by micro-$FeTiO_3$ powders (2.0 g) that were mixed thoroughly with ammonium bicarbonate (NH_4HCO_3, 0.67 g, served as pore-forming agent), and then the mixed powders were pressed (15 MPa in pressure) in a columnar module for

Fig. 1 **a** Schematic diagram of electrolysis apparatus and **b** optical photograph of the assembled ilmenite cathode
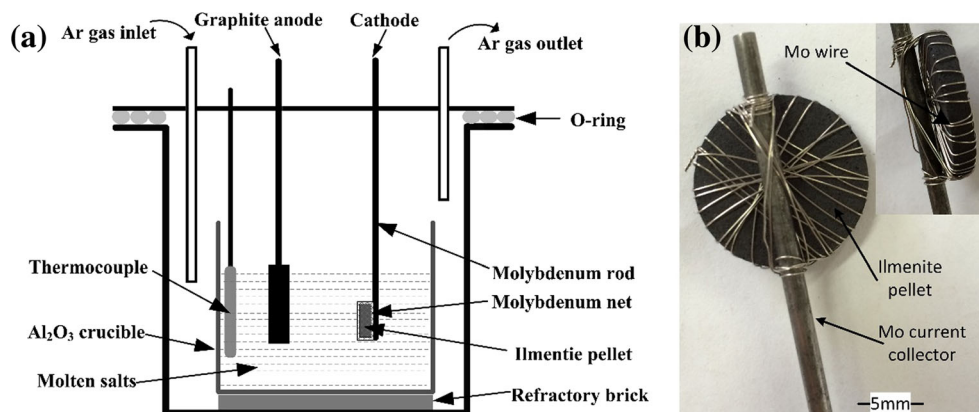
5 min to form a pellet of 13 mm in diameter and 3 mm in thickness. The mixed powders were further sintered in a numerical controlled tube furnace under argon inert atmosphere at 1173 K for 3 h. Finally, the pellet was wrapped with Mo wires to assemble as the cathode, as shown in Fig. 1b.

After electrolysis, the crucible was left to cool down in argon atmosphere. The reduced cathode was then lifted from the cooled salt and washed in distilled water for 3 h. The reduced pellet was then polished and analyzed by SEM, BSE, and EDS analysis (XL 30ESEM TMP model).

Results and discussion

Linear sweep voltammetry

The typical current-time plot was recorded during the 60 min of potentiostatic electrolysis of MCE with 0.006 g ilmenite powders at −1.5 V, as shown in Fig. 2, which indicated that the electrolytic current was sharply decreased from 0.132 to 0.02 A in the initial 5 min and maintained at about 0.02 A hereafter. In order to clarify the electrochemical behavior of ilmenite powders during the sharp current decrease stage as well as the further current stabilization periods, potentiostatic electrolysis was also respectively conducted at −0.8 V for
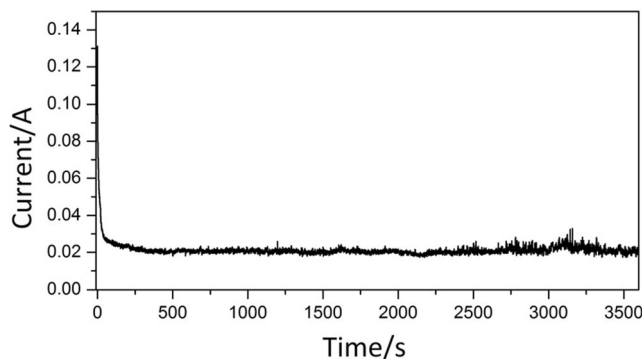

Fig. 2 Typical current-time curve during 60 min of potentiostatic electrolysis of $FeTiO_3$ powder at −1.5 V

5 min, 60 min and at −1.5 V for 5 min, 60 min. The products obtained were further analyzed by XRD, as shown in Fig. 3.
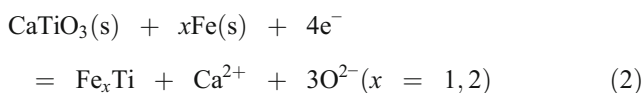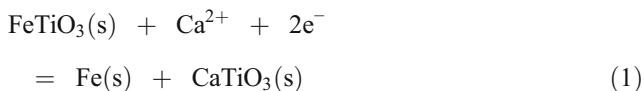
Figure 3 shows the phases transitions during the potentiostatic electrolysis of ilmenite in $CaCl_2$-NaCl molten salt. The detected diffraction peaks were also characterized with the crystal planes from the MDI Jade 9.0 software. From the XRD patterns of Fig. 3a, it was seen that after ilmenite powders were immersed into the melts for 5 h, there are no phase changes of them. All the detected diffraction peaks belong to the rhombohedral $FeTiO_3$ (PDF card #15-1203) with high intensity. The calculated lattice parameters of $FeTiO_3$ are a = 5.1202 Å, b = 5.1202 Å, c = 14.0229 Å, and V = 367.63 Å^3. After 5 min of electrolysis at −0.8 V, the ilmenite powders were reduced to $CaTiO_3$ with the largest peak intensity, minor intensities of Fe and $FeTiO_3$ phases, as seen in the XRD patterns of Fig. 3b, suggesting that ferrous oxide in ilmenite was quickly reduced to Fe and titanium dioxide in $FeTiO_3$ was transformed into $CaTiO_3$, leading to forming new diffraction peaks observed around 23.23°, 26.11°, 33.09°, 39.14°, 40.68°, 47.56°, 49.31°, 51.02°, 53.13°, 65.48°, and 82.04° that correspond respectively to the (110), (111), (112), (103), (022), (220), (221), (222), (131), (204), and (332) crystal planes of the intermediate $CaTiO_3$ (PDF card #22-0153), and forming three diffraction peaks at 44.67°, 65.02°, and 82.33° that correspond to the (110), (200), and (211) crystal planes of Fe (PDF card #88-2324). Take further observation in Fig. 3c, after 60 min of electrolysis at −0.8 V, the detected phases have been no changed but the peak intensity of $CaTiO_3$ is increased, implying the hard reduction of $CaTiO_3$ at −0.8 V.

The mixtures of FeTi, Fe_2Ti, Fe, and $CaTiO_3$ were detected after ilmenite was electrolyzed by 5 min and 60 min of electrolysis at −1.5 V, as shown in Fig. 3d, e. In cooperation with the detected phases in Fig. 3d, e, the peak intensity of $CaTiO_3$ at 33.09° is disappeared as the electrolysis time is prolonged, suggesting $CaTiO_3$ is reduced at −1.5 V. These electrolytic products, obviously, are indicative that ilmenite was preferentially reduced to the intermediates such as iron metal and perovskite via reaction (1) at small negative potentials, and

Fig. 3 XRD patterns of the reduced mixtures after potentiostatic electrolysis
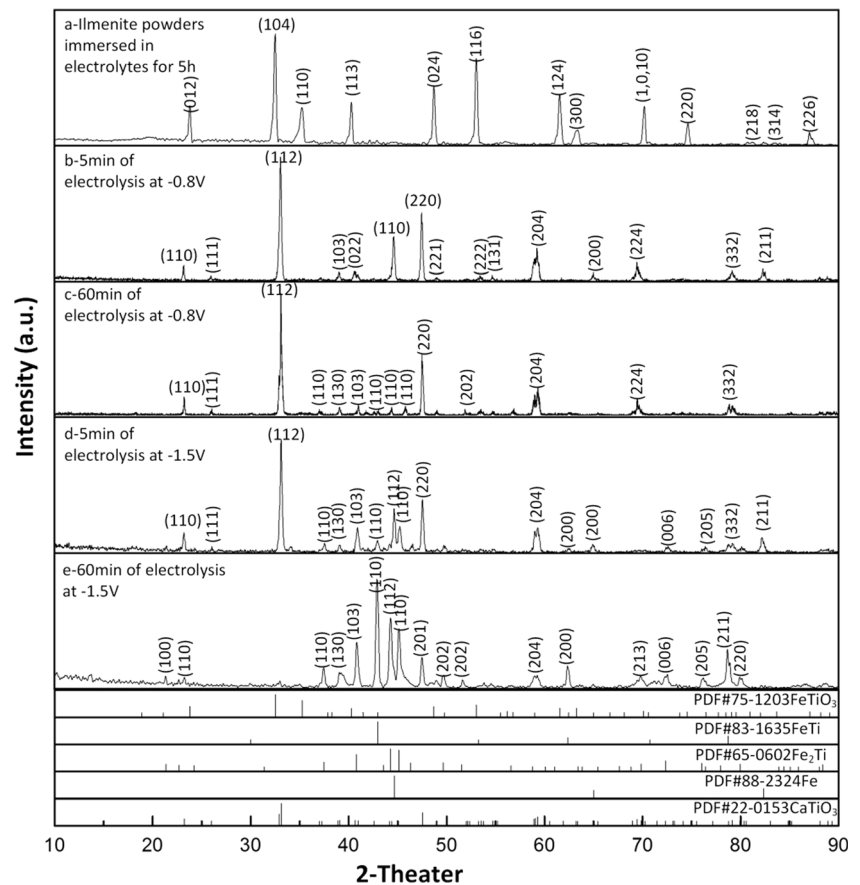
CaTiO$_3$ would be further reduced to ferrotitanium alloys in the presence of Fe metals at more negative potentials via reaction (2).

$$FeTiO_3(s) + Ca^{2+} + 2e^-$$
$$= Fe(s) + CaTiO_3(s) \quad (1)$$

$$CaTiO_3(s) + xFe(s) + 4e^-$$
$$= Fe_xTi + Ca^{2+} + 3O^{2-}(x = 1,2) \quad (2)$$

The electrochemical behavior of the mixtures partially reduced after potentiostatic pre-electrolysis was analyzed by the linear sweep voltammetry. In Fig. 4, curve a presented the cathodic polarization curve of metallic cavity electrode (MCE) without FeTiO$_3$ powders at a scan rate of 2 mV/s ranging from 0.05 to −1.6 V versus Ag wire in eutectic CaCl$_2$-NaCl melt at 973 K. It showed a small increasing current with negative potential scan. The polarization curve of FeTiO$_3$-MCE was then detected at the same condition, as shown in curve f. Compared to the blank MCE curve, a beginning reduction current at −0.05 V and some small but noticeable current peaks were observed in the scan range of potential, suggesting that the electrochemical deoxidization of ilmenite is a complex reduction of multi-steps.

The cathodic polarization features of the intermediate powders reduced respectively at −0.8 V for 5 min, 60 min and at −1.5 V for 5 min, 60 min were similar to those of ilmenite powders but the corresponding reduction current was lower than that of ilmenite, as shown in curves b ~ e. According to the phases detected in Fig. 3, curve b and e represented the cathodic polarization features of the mixture powders of
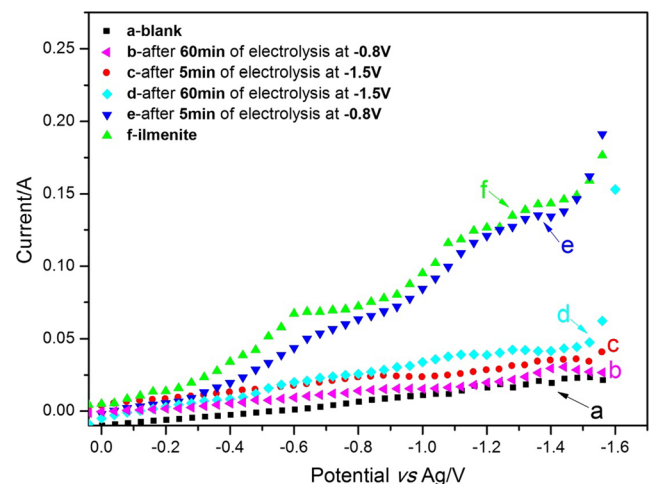

Fig. 4 Cathodic polarization curves of MCE with/without ilmenite powder and partially reduced mixtures after pre-potentiostatic electrolysis in molten salt

$FeTiO_3$, Fe, and $CaTiO_3$; and curves c and d recorded the polarization curve of the mixture powders of $CaTiO_3$, Fe, FeTi, and Fe_2Ti. It showed the beginning reduction current near −0.05 V and the increasing current with the negative potential scan in curve e, but in curves b ~ d; the reducing current was increased slightly as the potential scanned negatively in the same conditions. The reducing current in curves b ~ d were obviously lower than that in curve e, suggesting that the reduction of $CaTiO_3$ would become more and more difficult than that of $FeTiO_3$ as the electrolysis constantly progresses, resulting in the slower reduction kinetics. The reason could be attributed to the fact that $FeTiO_3$ is more easily reduced than $CaTiO_3$ in thermodynamics, resulting in the two-step deoxidization that is the first easy deoxidization of $FeTiO_3$ and the further difficult reduction of $CaTiO_3$.

Constant cell voltage electrolysis

Based on the previous study of linear sweep voltammetry, in order to better understand the electrochemical reduction behavior of ilmenite, the sintered ilmenite pellet was also studied via eutectic $CaCl_2$-NaCl melt electrolysis in a two-electrode system by using an assembled ilmenite pellet electrode as cathode and graphite as anode with cell voltage of 3.2 V at 973 K. The partially reduced pellets after electrolysis for 2, 6, 12, and 16 h were washed in distilled water and manually grounded into powders for XRD phase detection, as shown in Fig. 5. It showed clearly that the electrolytic products were FeTi, Fe_2Ti, $CaTiO_3$, and Fe phases for the ilmenite pellet reduced for 2 h. The presence of the intermediate product

$CaTiO_3$ presented the highest diffraction peak intensities at 33.12° with the following 37.33°, 33.89°, 40.66°, 47.54°, 78.78°, 80.37°, and 82.22°, respectively corresponding to the (112), (120), (110), (103), (220), (213), (211), and (311) crystal planes. The lattice parameters of the orthorhombic $CaTiO_3$ are $a = 5.1773$ Å, $b = 7.8864$ Å, $c = 5.3022$ Å, and $V = 216.49$ Å^3. Besides, the formation of $CaTiO_3$ also suggested that calcium ions in molten salt participated in the electrochemical reduction of ilmenite, obviously, implying that ilmenite was not directly reduced to ferrotitanium alloy. In the mixtures reduced for 6 and 12 h, FeTi became the major product, while Fe_2Ti, Fe, and $CaTiO_3$ were the minor phases. After 16 h of electrolysis, from Fig. 5(e_0), only three well-defined diffraction peaks appearing at 43.10°, 62.49°, and 78.76° were observed in the XRD patterns, which could be indexed into the lattices of (110), (200), and (211) crystal planes of the FeTi (PDF card #83-1635) with Pm-3m space group of the cubic crystal system. The lattice parameters of FeTi calculated are $a = 2.9793$ Å, $b = 2.9793$ Å, $c = 2.9793$ Å, and $V = 26.44$ Å^3. No other diffraction peaks were detected, suggesting the high purity of the production of FeTi powders. In addition, the product evolutions strongly suggest the fact that $CaTiO_3$ is further deoxidized and simultaneously reacted with the intermediates Fe, Fe_2Ti to form FeTi. The result is also in good agreement with those conducted by the $FeTiO_3$-MCE potentiostatic electrolysis.

After electrolysis terminals, the reduced pellets were cut in cross-sections and polished by sandpaper to analyze the cross-section by use of back-scattered electron imaging (BSE) and then were manually grounded in powders to observe the
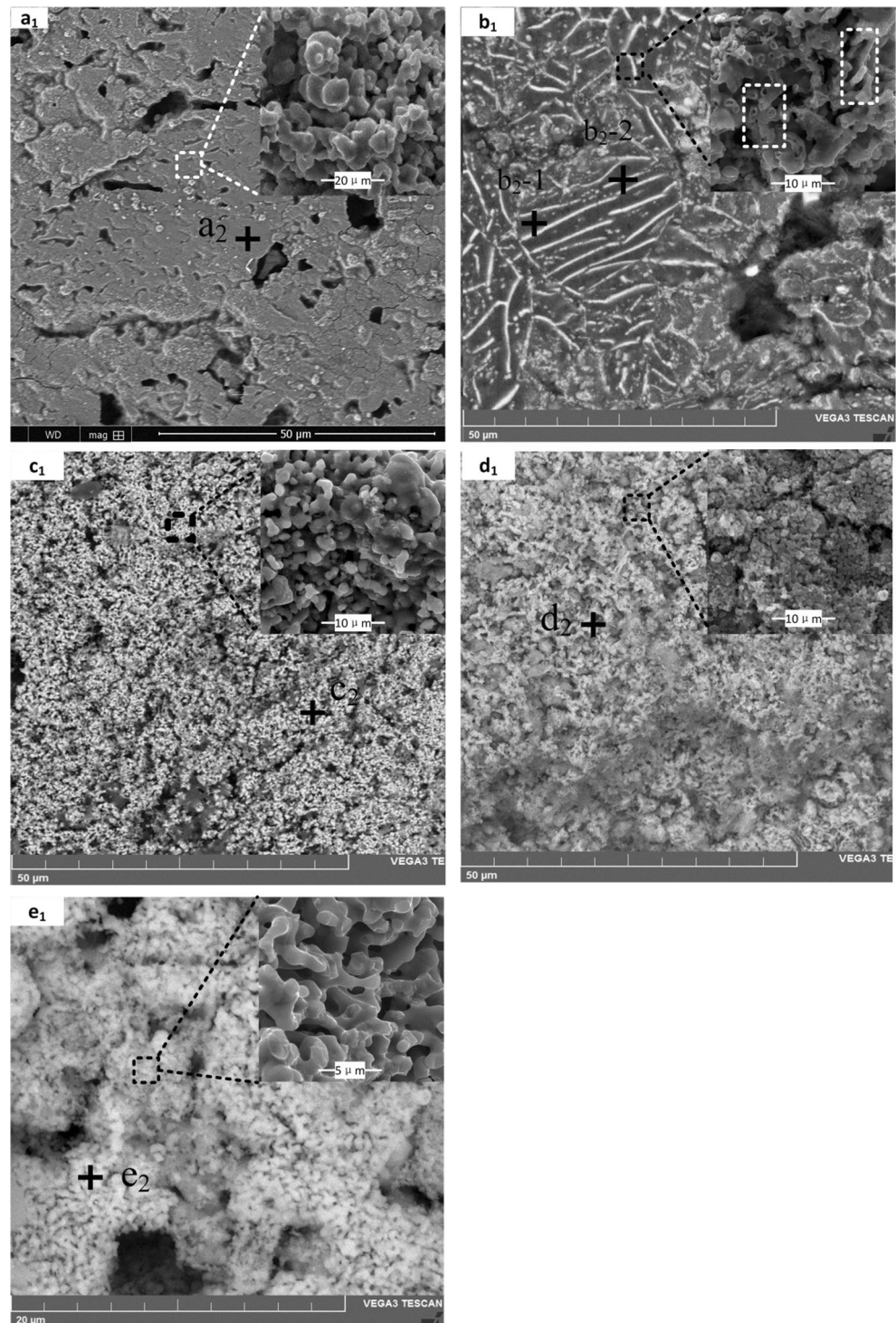
Fig. 5 XRD patterns of the mixtures before (a_0) and after electrolyzed for 2 h (b_0), 6 h (c_0), 12 h (d_0), and 16 h (e_0)
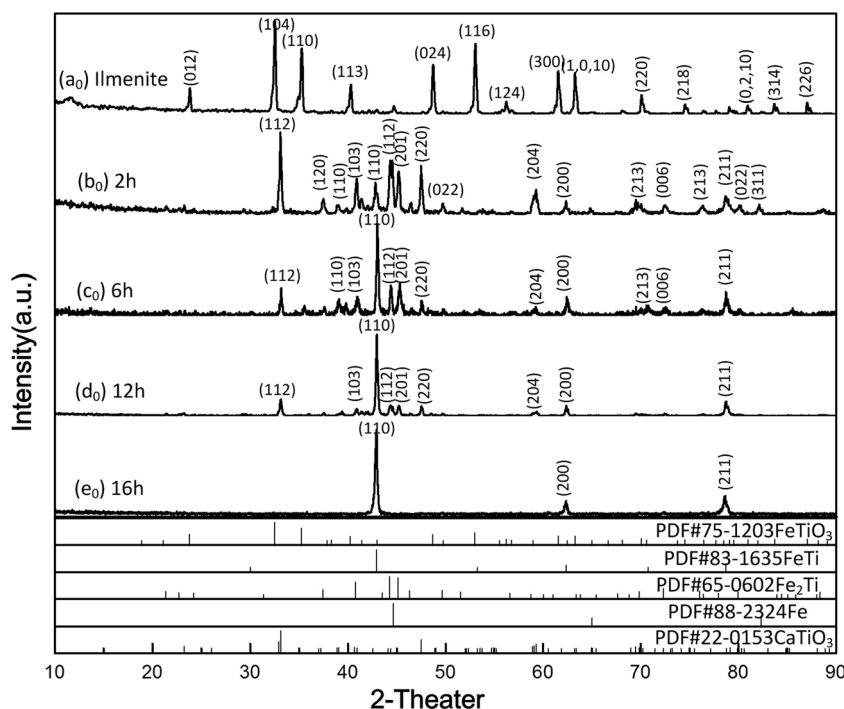
partially enlarged area by scanning electron microscopy (SEM), as shown in Fig. 6. The elemental content was also detected by energy-dispersive spectroscopy (EDS), as shown in Fig. 7. The micrograph of ilmenite pellet after immersed into $CaCl_2$-NaCl melt and washed in distilled water was presented in Fig. 6a$_1$. It showed that ilmenite particles with dense structures have a size of about 15 μm in diameter and some

pores with about 5 μm in diameter exist inside the pellet. These pores, to a great extent, play an important role for the penetration of electrolyte into the core of ilmenite pellet as well as oxygen transfer from solid oxides into electrolyte. After 2 h of electrolysis, the reduced pellets showed the light gray phases surrounded by white spiculate matrix. According to the EDS analysis in Fig. 7b$_2$ and XRD results in Fig. 5b$_0$,

Fig. 6 The cross-section back-scattering micrographs with the corresponding partially enlarged second-electron scattering micrographs inside after different reduction period: unreduced ilmenite by immersed in the electrolyte (a$_1$); electrolyzed for 2 h (b$_1$); 6 h (c$_1$); 12 h (d$_1$); and 16 h (e$_1$)
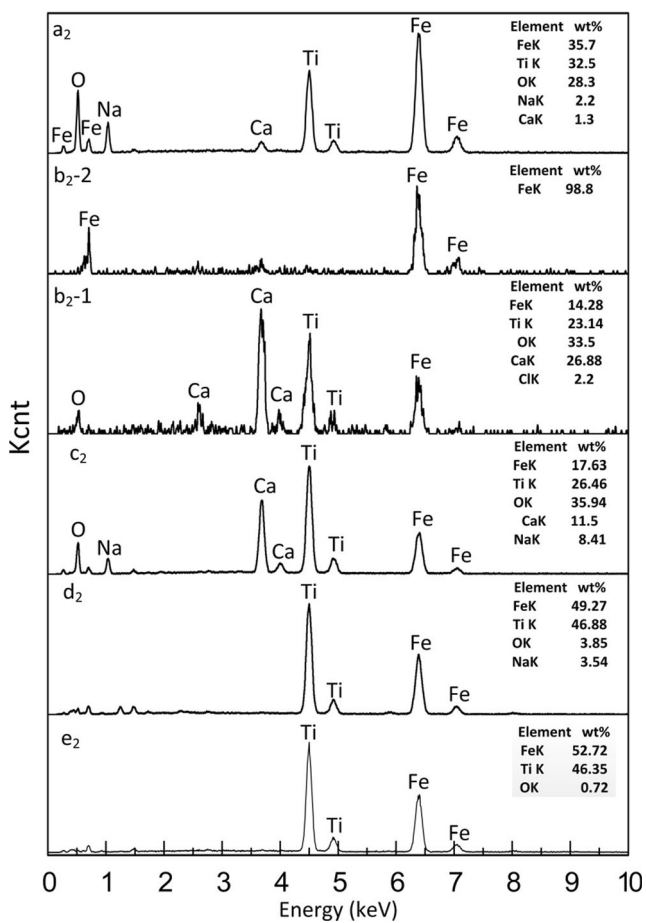
Fig. 7 EDS results of the partially reduced ilmenite; the detected element contents inside correspond to the detected area in Fig. 6

will be further deoxidized in the presence of these increasing iron grains to form ferrotitanium alloys. Moreover, pores that are formed during the deoxidization process could continually enlarge the boundary areas where the oxide particles and electrolyte are in contact and can definitely promote the ionized oxygen transport. Take further inspection in Fig. $6b_1$, due to the extensively high reduction rate in the early electrolytic process, the newly produced iron grains were generated to form nodular nucleuses near pores and clusters rather than continuous layers inside the pellet. The enriched metallic matrix could increase the conductivity of the pellet and could also serve as the conducting medium to enhance the reduction process from the superficial to the profound propagation.

By furthering electrolysis time to 6 h, the morphology of the reduced particles in Fig. $6c_1$ showed the light white grains covering the surface with a content of 17.63 mass% Fe, 26.46 mass% Ti, 11.5 mass% Ca, and 35.94 mass% O, suggesting a combined component of Fe_2Ti, FeTi, and $CaTiO_3$ mixtures, as were evidenced by XRD results in Fig. $5c_0$. Moreover, the reduced pellet showed more porous and looser structures instead of the dense pellet. This could be ascribed to the further deoxidization of the solid intermediate $CaTiO_3$ and the release of oxygen from the solid crystals towards the pores. The SEM image inside Fig. $6c_1$ showed that the white metallic particles of 2 μm were adhered to the larger solid dark gray particles of 10 μm. In this process, the spiculate iron phases and the dense perovskite phases were lost simultaneously, suggesting that perovskite was deoxidized near iron metals to form metallic ferrotitanium alloys.

After 12 h of electrolysis, the white grains grew up to about 3 μm in content of 49.27 mass% Fe, 46.88 mass% Ti, and 3.85 mass% of O, as listed in Fig. $7d_2$. The surface presented a regular porous and loose structure. From the SEM image inside Fig. $6d_1$, it could find the newly formed ferrotitanium grains in homogeneous structures. As the newly formed crystals grew up and the deoxidization proceeded, the final content after 16 h of electrolysis contained the porous ferrotitanium powder less than 5 μm with 52.72 mass% Fe, 46.35 mass%
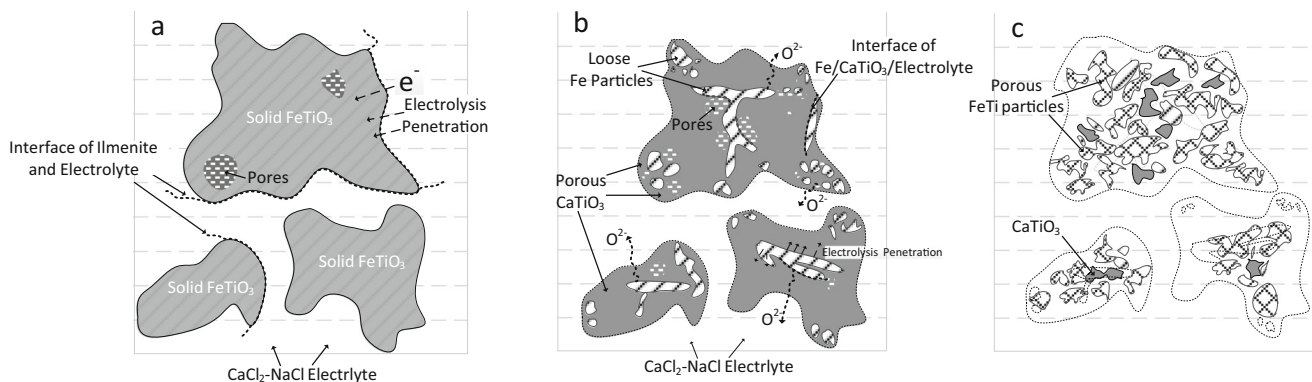
the white spiculate phases were the enriched Fe metals of 98.8 mass%, and the light gray phases were the $CaTiO_3$. The composition of mixtures of $CaTiO_3$, Fe_2Ti, and FeTi was 14.28 mass% Fe, 23.14 mass% Ti, 33.5 mass% O, 26.88 mass% Ca, and 2.2 mass% Cl. The SEM image inside showed the dendritic metallic iron grains and newly produced pores, implying that with the constant growth of metallic iron grains, the initial dense perovskite particles

Fig. 8 Schematic illustration derives from the initial ilmenite particles to the final formation of porous ferrotitanium alloys

Ti, and 0.72 mass% O, as shown in Fig. 7e$_1$. Thus, the morphology evolutions at different electrolysis terminals suggest that the deoxidization process includes the iron grain increase, the deoxidization of solid intermediate $CaTiO_3$ near the spiculate iron phases, and the increase in pores and ferrotitanium alloying process.

Mechanism of electrochemical reduction

According to the above analysis, the schematic illustration of the ilmenite electrolytic process is proposed in Fig. 8. As shown in Fig. 8a, the electrons are transmitted from the cathode current collector to the surface of ilmenite particles via the pores. By applied overpotential, ilmenite is reduced first to form Fe metals and $CaTiO_3$ at the interface between the solid particles and $CaCl_2$-NaCl electrolyte via reaction (1), as illustrated in Fig. 8b. The newly formed iron grains then grow up and are enriched to form nodular nucleuses, that is, to form clusters morphologically near the pores and dendritic grains inside the pellet. These enriched metals act as the conducting medium to increase the pellet conductivity and enhance the electron transport.

Simultaneously, the intermediate $CaTiO_3$ starts to be deoxidized as the reduction process penetrates inward. However, due to the slow deoxidization rate of perovskite, the electrolysis proceeds slowly. In this process, $CaTiO_3$ particles are suggested to be reduced near Fe-enriched clusters to Fe_2Ti and FeTi via reaction (2), as illustrated in Fig. 8c. As the deoxidization proceeds constantly, the dense pellet turns to be more porous and separates many trivial ferrotitanium grains. After electrolysis, ilmenite is finally reduced to porous FeTi.

Overall, the electrochemical deoxidization actually occurs in the next two stages. First, ilmenite is reduced to $Fe/CaTiO_3$ mixtures; second, the intermediate $CaTiO_3$ is directly deoxidized to produce ferrotitanium alloys, mainly Fe_2Ti and FeTi near Fe-enriched phases. The ionized oxygen released from the solid state is then dissolved into the electrolyte, diffused to the anode by electric field force, and discharged at the graphite consumable anode in the form of CO/CO_2 via reaction (3).

$$yO^{2-} + C(s)\text{-}2ye^- = CO_y(g)(y = 1, 2) \qquad (3)$$
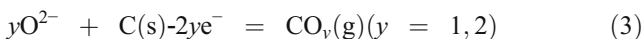
Conclusions

(1) The linear cathodic sweep voltammetry of $FeTiO_3$ powders in MCE shows that the direct electrochemical reduction is a complex heterogeneous process since some intermediates such as Fe, $CaTiO_3$, and Fe_2Ti have been found. The reduction of $CaTiO_3$ would become more and more difficult than that of $FeTiO_3$ as the electrolysis

constantly progresses, resulting in the slower reduction kinetics. The reason could be attributed to the fact that $FeTiO_3$ is more easily reduced than $CaTiO_3$ in thermodynamics, resulting in the two-step deoxidization that is the first easy deoxidization of $FeTiO_3$ and the further difficult reduction of $CaTiO_3$.

(2) Constant cell voltage electrolysis in two electrodes system has also been applied to analyze the phase transformation. The result shows that $FeTiO_3$ is not directly reduced to FeTi. Instead, $FeTiO_3$ is first reduced to form Fe metals and $CaTiO_3$ particles. $CaTiO_3$ is further deoxidized and simultaneously reacts with the intermediates such as Fe, Fe_2Ti to produce FeTi. The pre-formed Fe and Fe_2Ti phases could surely increase the pellet conductivity and will act as the charge transfer medium to enhance the reduction process penetrating inward.

(3) Pores within ilmenite pellets play an important role for the penetration of electrolyte and provide transport path for the oxygen ions from solid oxides into electrolyte. During the reduction, the dense solid pellet turns to be porous continually, and more pores could be found inside the particles. Thus, after deoxidization, micro-ferrotitanium alloy powders are formed.

References

1. Tan S, Örs T, Aydinol MK, Öztürk T, Karakaya İ (2009) J Alloy Compd 475:368–372
2. Wang D, Jin X, Chen GZ (2008) Annu Rep Prog Chem Sect C 104:189–234
3. Zou X, Lu X, Zhou Z, Xiao W, Zhong Q, Li C, Ding W (2014) J Mater Chem A 2:7421–7430
4. Descallar-Arriesgado RF, Kobayashi N, Kikuchi T, Suzuki RO (2011) Electrochim Acta 56:8422–8429
5. Abdelkader AM, Kilby KT, Cox A, Fray DJ (2013) Chem Rev 113:2863–2886
6. Xiao W, Jin X, Deng Y, Wang D, Hu X, Chen GZ (2006) ChemPhysChem 7:1750–1758
7. Shi X, Jin X, Xiao W, Hou X, Chen H, Chen GZ (2011) Chem-Eur J 17:8562–8567
8. Xu Y, Jiang H, Li X, Xiao H, Xiao W, Wu T (2014) J Mater Chem A 2:13345–13351
9. Kai J, Hu X, Ma M, Dihua W, Guohong Q, Xianbo J, Chen GZ (2006) Angew Chem Int Edit 45:428–432
10. Chen GZ (2015) Miner Process Extr M 124:96–105
11. Fray DJ (2001) JOM 53:27–31
12. Liu X, Hu M, Bai C, Lv X (2014) High Temp Mater-Isr 33:377–383
13. Rong L, He R, Wang Z, Peng J, Jin X, Chen GZ (2014) Electrochim Acta 147:352–359
14. Hu M, Bai C, Liu X, Lv XI, Du J (2011) J Min Metall B 47:193–198
15. Li G, Jin X, Wang D, Chen GZ (2009) J Alloy Compd 482:320–327

16. Panigrahi M, Lizuka A, Shibata E, Nakamura T (2013) J Alloy Compd 550:545–552
17. Chen ZY, Chou KC, Li FS (2013) J Manufac Sci Pro 13:127–131
18. Panigrahi M, Shibata E, Lizuka A, Nakamura T (2013) Electrochim Acta 93:143–151
19. Castrillejo Y, Martínez AM, Haarberg GM, Børresen B, Osen KS, Tunold R (1997) Electrochim Acta 42:1489–1494
20. Yan XY, Fray DJ (2005) J Electrochem Soc 152:D12–D21
21. Xiao W, Jin X, Chen GZ (2013) J Mater Chem A 1:10243–10250
22. Wang T, Gao H, Jin X, Chen H, Peng J, Chen GZ (2011) Electrochem Commun 13:1492–1495
23. Wu T, Xiao W, Jin X, Liu C, Wang D, Chen GZ (2008) Phys Chem Chem Phys 10:1809–1818
24. Dring K, Dahswodd RD, Inman D (2005) J Electrochem Soc 152: E104–E113
25. Osarinmwian C, Roberts EPL, Mellor IM (2015) Chem Phys Lett 621:184–187
26. Wang D, Qiu G, Jin X, Hu X, Chen GZ (2006) Angew Chem Int Edit 45:2384–2388
27. Xiao W, Wang D (2014) Chem Soc Rev 43:3215–3228